Microphase Separation in Thin Films of Poly(styrene-block-4-vinylpyridine) Copolymer2-(4`-Hydroxybenzeneazo)benzoic Acid Assembly

7 AUTHORS, INCLUDING:

Alexander Sidorenko
University of the Sciences in Philadelphia
53 PUBLICATIONS **2,083** CITATIONS

Microphase Separation in Thin Films of Poly(styrene-*block*-4-vinylpyridine) Copolymer−2-(4′-Hydroxybenzeneazo)benzoic Acid Assembly

Igor Tokarev,[†] Radim Krenek,[†] Yevgen Burkov,[‡] Dieter Schmeisser,[‡] Alexander Sidorenko,*,[†] Sergiy Minko,[§] and Manfred Stamm[†]

Institut für Polymerforschung Dresden, Hohe Strasse 6, 01069 Dresden, Germany, Brandenburgische Technische Universität Cottbus, Universitätsplatz 3-4, 03046 Cottbus, Germany, and Department of Chemistry, Clarkson University, Potsdam, New York 13699-5810

ABSTRACT: The fine structure of thin films of poly(styrene-*block*-4-vinylpyridine) copolymer−2-(4′-hydroxybenzeneazo)benzoic acid (PS-PVP+HABA) assembly has been studied using the combination of atomic force microscopy, ellipsometry, X-ray reflectivity, GISAXS, XPS, and XPEEM. The films consist of cylindrical nanodomains formed by PVP+HABA associates surrounded by PS matrix. Alignment of the domains can be switched upon exposure to vapors of different solvents from the parallel to perpendicular orientation and vice versa with respect to the surface plane. Swelling in 1,4-dioxane leads the system from the cylindrical to the spherical morphology. Solvent evaporation results in a shrinkage of the matrix in the vertical direction and subsequent merging of the spheres into the perpendicularly aligned cylinders. The cylinders form a regular hexagonal lattice with a spatial period of 25.5 nm. On the other hand, vapors of chloroform induce in-plane alignment. The films consist of parallel layers of the cylinders separated by PS matrix and demonstrate the fingerprint-like structure. The nanocylinders of PVP+HABA are packed into a distorted hexagonal lattice exhibiting 31 nm in plane and 17 nm vertical periodicity. In both cases a thin wetting layer is found at the polymer−substrate interface. The free surface is enriched with PS.

Introduction

Block copolymers (BC) are able to form periodic nanostructures due to the immiscibility of unlike polymer blocks. The morphology depends on the volume ratio of the blocks, while the size of the features, typically on the range of tens of nanometers, is mostly influenced by the length of the blocks.[1−3] The microphase separation makes them promising for a number of applications in nanoscience and technology.

Four typical morphologic patterns are observed for diblock copolymers in bulk: spherical (body-centered cubic), cylindrical *C* (hexagonal), gyroidal (bicontinuous cubic), and lamellar.[1] However, the situation becomes more complicated for thin block copolymer films. The anisotropy is an attribute of thin films. It forces us to distinguish also the orientation of the BC patterns with respect to the direction normal to the surface plane. Thin films of BC are confined between two interfaces. The interfacial energy plays a crucial role in orientation and ordering in thin BC films. The preferential wetting of the substrate with one of the phases drives the system to the parallel alignment of nanodomains. In addition, the lowest surface tension component occupies the free surface of polymer film, enhancing the trend toward parallel alignment. The preferential wetting was first observed for symmetric BCs with lamellar structure[4−6] and later extended to hexagonal cylindrical[7−10] and BCC (body-centered cubic) spherical[11,12] morphologies. The

parallel alignment of BC nanodomains usually results in terracing of the free surface of BC films. It arises from the incommensurability of the bulk period with the film thickness.[13] A mismatch between the BC film thickness, *d,* and lamellar or interlayer period, *L,* results in the formation of holes or islands. As a result, the thickness of BC film is quantized according to *L*. The quantization condition depends on whether the same block forms wetting layers at the film interfaces (symmetric wetting) or different blocks (asymmetric wetting). The thickness of the symmetric BC films with the lamellar morphology is quantized to values of nL and $(n + 1/2)L$ for the symmetric and asymmetric wetting cases, respectively, where *n* is an integer.[14,15] The quantization relation for poly(styrene-*block*-2-vinylpyridine) (PS-*b*-P2VP) films of the *C* morphology with asymmetric wetting of the interfaces found by Liu et al.[9] is a bit more complicated and expressed as $d = (n + \alpha)L + \beta$, where α is the fractional thickness of the first top cylindrical layer and β is the thickness of the lamellar layer adjacent to the substrate interface. The terrace formation leads to an increase of the film surface and, subsequently, free energy of the system. Magerle et al.[16] found that depending on the film thickness, instability of the system may result in perpendicularly aligned cylinders as well as wetting layers, perforated lamellae, and other structures. Thus, there are some methods to overcome the preferential wetting and approach a desired orientation in BC thin films.

The orientation is the most important in the case of cylindrical and lamellar morphologies. Sufficient effort has been addressed to control the orientation of the nanoscopic domains in thin films. An external electric field applied to BC samples induces alignment of cylinders or lamellas.[17−22] The difference in the dielectric

* To whom correspondence should be addressed. Phone: +49 (0351) 4658271. Fax: +49 (0351) 4658284. E-mail Sydorenko@ipfdd.de.
[†] Institut für Polymerforschung Dresden.
[‡] Brandenburgische Technische Universität Cottbus.
[§] Clarkson University.

constant of unlike blocks is a driving force for the alignment. The nanodomains tend to orient along the electric field lines, lowering the free energy of the system. The field-induced alignment has been used to obtain both parallel and perpendicular orientation in melt as well in solution.[23] Also, the effect of the preferential wetting can be minimized using the "neutral surface" approach. The substrate surface was modified by the grafting of random copolymer brush constituted of the same monomers as BC.[24] The perpendicular orientation of cylindrical domains in poly-(styrene-*block*-methyl methacrylate) thin film was obtained using this approach. A solvent-induced orientation was demonstrated by Kim and Libera[25] and recently convincingly proved by Russell et al.[26] They investigated swollen thin films of BC and found that fast solvent evaporation may induce the perpendicular alignment of minor block cylinders with respect to the sample surface, while slow evaporation results in parallel alignment due to the preferential wetting.

Recently, it was demonstrated that well-ordered nanostructures may be fabricated in bulk not only from block copolymers but also from supramolecular assemblies of low molar mass additives and block copolymers (SMA).[27,28] Recently, we reported the synthesis of the SMA from poly(styrene-*block*-4-vinylpyridine) (PS-PVP) and 2-(4′-hydroxybenzeneazo)benzoic acid (HABA). HABA selectively associated with pyridine nitrogen of PS-PVP via hydrogen bonding and formed SMA. Thin films of the SMA demonstrated well-ordered hexagonal cylindrical morphology. The nanodomains were formed by the PVP+HABA associates surrounded by the PS matrix.[29] The ordered thin films were obtained via spin or dip coating without additional annealing. Depending on the solvent, the assembly adopted either a perpendicular (SMA⊥) or a parallel (SMA∥) cylinder alignment with respect to the film surface plane. The procedure was shown to be very fast and simple. The reorientation is reversible. Swelling of SMA in vapors of the corresponding solvent leads to sufficient improvement of the ordering. We explained the observed behavior by the specific intermolecular aggregation of HABA molecules which can overcome the effect of confining surfaces and stabilize the perpendicular alignment in 1,4-dioxane due to the self-adaptive behavior of SMA surface.

Extraction of HABA with selective solvent results in a porous block copolymer (PBC) film. Depending on the cylinder alignment we obtain PBC in two forms. The perpendicular cylinder alignment results in a nanomembrane, denoted further as PBC⊥, with a hexagonal lattice (24.5 ± 0.5 nm in the period) of hollow channels ca. 8 nm in diameter. SMA with the parallel cylinder alignment can be turned into PBC∥ with a "fingerprint" surface. The walls of the nanochannels or grooves are formed by the reactive PVP brush.

In this paper we investigate the fine details of microphase separation in thin films of the poly(styrene-*block*-4-vinylpyridine)−HABA assembly. The structure of SMA and PBC thin films of both perpendicular and parallel alignment is studied by scanning probe microscopy, ellipsometry, X-ray reflectivity, GISAXS, XPS, and μNEXAFS.

Experimental Section

Materials. Poly(styrene-*block*-4-vinylpyridine) (PS-PVP), with number-averaged molecular masses (M_n) of PS 35 500 g/mol, PVP 3680 g/mol, $M_w/M_n = 1.06$ for both blocks, was purchased from Polymer Source, Inc. 2-(4′-Hydroxybenzene-

azo)benzoic acid (HABA) was purchased from Sigma-Aldrich. Solvents−1,4-dioxane, chloroform, THF, toluene, methanol, and dichloromethane−were purchased from Acros Organics and used as supplied. Silicon wafers {100} and quartz slides were cleaned successively in an ultrasonic bath (dichloromethane) for 15 min and "piranha" bath (30% H_2O_2, 70% of H_2SO_4, *chemical hazard*) for 40 min at 82 °C and then thoroughly rinsed with Millipore water and dried in argon flow.

Fabrication of Nanomembranes/Nanotemplates. PS-PVP and HABA (1 mol of HABA and 1 mol of 4-vinylpyridine monomer unit) were dissolved separately in 1,4-dioxane. PS-PVP solution was slowly added dropwise to HABA solution while heating to 95 °C in an ultrasonic bath. The elevated temperature during mixing was very important for reproducible formation of SMA. The resulting solution (range of the total concentration of PS-PVP + HABA from 0.3 to 1 wt %, fraction of HABA 17.8 wt %) was kept at least overnight to complete hydrogen-bond formation. Thin films were prepared by dip coating from the filtered (200 nm pore size PTFE filter) solutions. Dip coating was performed with rates ranging from 0.1 to 0.5 mm s^{-1}. An additional vapor annealing of a thin film of SMA⊥ samples in 1,4-dioxane was applied to improve the order of nanodomains. Alternatively, the samples dip-coated from 1,4-dioxane solution were treated in vapors of chloroform to arrange parallel alignment of the nanodomains. In both cases a swelling ratio of ca. 2.75 (room temperature) of the SMA films was reached, as visually estimated from the color of the swollen films. Immediately afterward the swelling chamber was opened, and solvent was allowed to freely evaporate; both chloroform and 1,4-dioxane evaporated within a fraction of a second. PBC samples were fabricated by selective extraction of HABA with methanol.

The PS-PVP copolymer exhibits spherical morphology in bulk when the structure is formed by PVP core surrounded by PS shell.[30] From the SAXS experiments we found that the PS-PVP+HABA equimolar assembly produces the hexagonal cylindrical bulk structure with a wave vector of 0.237 nm^{-1}, which corresponds to 26.5 nm in period hexagonal structure.

Characterization of the Ordered Thin Films. The thickness of the polymer films was measured by a SE400 ellipsometer (SENTECH Instruments GmbH, Germany) with a 632.8 nm laser at a 70° incident angle. The pore fraction of the thin polymer films was estimated from the effective refractive index (n, measured with ellipsometry) using Bruggeman's effective-medium approximation equation[31]

$$(1 - \nu)((\epsilon_1 - \epsilon_e)/(\epsilon_1 + 2\epsilon_e)) + \nu((\epsilon_2 - \epsilon_e)/(\epsilon_2 + 2\epsilon_e)) = 0 \quad (1)$$

where ϵ_i and ϵ_e are the dielectric constants of the ith component and the effective dielectric constant, respectively, and ν is the volume fraction of the second component of the film. The relationship between n and ϵ is given by $n_i^2 = \epsilon_i$.

X-ray reflectivity was measured with a X-ray diffractometer XRD 3003 T/T (Seifert-FPM, Freiberg, Germany). The operating wavelength was 1.54 Å^{-1} (Cu Kα). The experimental data were analyzed by fitting of the measured reflectivity curves. Multilayer models were applied for the fitting. Refractive indices and the thickness of each layer and interfacial roughness were used as fitting parameters. The fitting was performed with Parratt32, ver. 1.5, which realizes the Parratt's recursive method for rough interfaces.[32]

X-ray photoelectron emission microscopy (XPEEM) and near-edge X-ray absorption fine structure (NEXAFS) spectroscopy measurements were performed on the U49/2-PGM2 beamline at the BESSY-II synchrotron radiation facility.[33] Details of the electron spectrometer used and the beamline parameters are published elsewhere.[34] The spectromicroscopic characterization by XPEEM was performed with a FOCUS-IS PEEM (Omicron). The setup was equipped with a CCD camera. The camera total intensity is used to record the NEXAFS signal which is used to obtain pixel-resolved local spectroscopic information from the XPEEM images (μ-NEXAFS). The setup was also used to record X-ray photoelectron spectra (XPS) for quantitative analysis of N, O, C, and Si

species in the film and at the interface with SiO_2. XPS spectra of the samples were acquired setting C1s and N1s windows. To determine the element ratio, normalized peak areas (Ω) were calculated from initial peak areas (raw area Φ, counts per second) of the survey spectra according to eq 2[35]

$$\Omega = \Phi/(RSF \times tx) \qquad (2)$$

where RSF is the respective sensitivity factor and tx is the spectrometer's transmission function.

To evaluate the chemical composition of the grafted layer, we used the ratios of nitrogen and carbon atoms $\varphi_{N1s/C1s}$ obtained experimentally and compared them with the values calculated for the case of uniformly distributed components.

The difference between the element distribution at the interface and in depth (down to 8 nm) was investigated varying the angle θ between the normal to the sample surface plane and the analyzer entrance. At $\theta = 0°$, the signal from the "depth" is maximized compared to that from the surface layer. At small angles the signal from the surface becomes strongly enhanced compared to that from the bulk. The preferential location of the atoms can thus be estimated from analysis of the ratio between pick intensities recorded for different atoms as a function of θ.[36]

Atomic force microscopy (AFM) imaging was performed using a Dimension 3100 scanning force microscope (Digital Instruments, Inc., Santa Barbara) and a CP microscope (Park Scientific Instrument, Inc) in the tapping mode. The tip characteristics are as follows: spring constant $1.5-3.7$ N m^{-1}, resonant frequency $45-65$ Hz, tip radius ca. 10 nm. Analysis of the AFM images (fast Fourier transform and power spectral density) was performed with WSxM software (Nanotec Electronica).

Grazing incidence small-angle X-ray scattering (GISAXS) measurements were performed at the beamline BW4 of Hamburg Synchrotron Radiation Laboratory (HASYLAB) at Deutsches Elektronen-Synchrotron (DESY). White synchrotron radiation was monochromatized to 1.38 Å. Two-circle goniometers with a z-transition table were used for the reflection mode. The sample–detector distance was 2.21 m. The 2D patterns of the scattered intensity were recorded with a detector consisting of a 512×512 pixels array. A beam stop was installed in the position of the reflected beam to block spillover of intense specular radiation in the scattering plane.

Results

Parallely Aligned C Morphology. We start consideration of the fine structure of thin block copolymer assembly films with the parallely aligned *C* morphology. The parallel alignment of the minor block cylinders and lamellae is common for most of block copolymers due to the effect of preferential wetting and well described in the literature.[4–12]

We performed a series of X-ray reflectivity measurements of the parallely aligned sample before (SMA∥) and after HABA extraction (PBC∥). The reflectivity curves were acquired in the same location to ensure correspondence of the samples. The resulting reflectivity curves and profiles of electron density are shown in Figure 1. A low electron density contrast between PS and PVP prohibits resolving the fine vertical structure of SMA. Addition of HABA makes no changes in the contrast. The reflectivity data were fitted using a single-layer model with an electron density ρ of ca. 9.5×10^{-6} Å^{-2}. This value corresponds to the density of both PS and PVP.[37] However, extraction of HABA leads to a drastic transformation of the reflectivity curve and the corresponding density profile. In view of a complex profile of PBC∥ (Figure 1b) it is worth noting that any attempts to simplify the model profile or introduce an additional layer were unsuccessful. As expected, two strata of low density of ca. 7.2×10^{-6} Å^{-2} are clearly
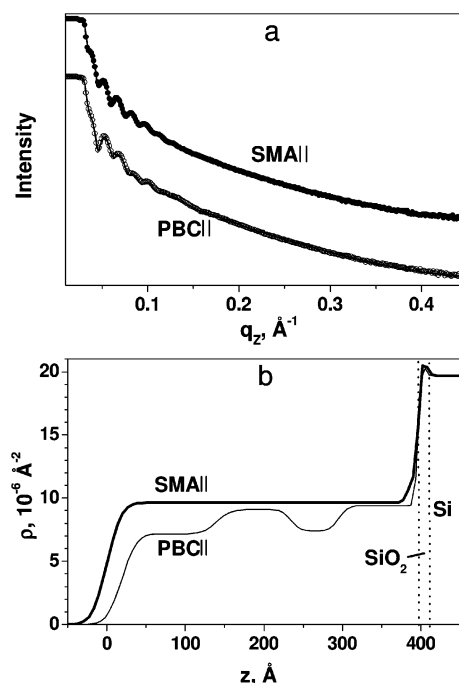
Figure 1. Measured (circles) and simulated (solid lines) X-ray reflectivity of SMA∥ (filled circles) and PBC∥ (open circles) films (a), and profiles of electron density ρ corresponding to the fit for SMA∥ (thick line) and PBC∥ (thin line) (b).

Table 1. Ellipsometry Data of Typical Samples of SMA with Parallel and Perpendicular Cylinder Alignments Before and After HABA Extraction

	refractive index n	effective porosity	thickness, nm	thickness loss upon washing, %
SMA∥	1.616		40.1	
PBC∥	1.523	0.111	37.5	6.5
SMA⊥	1.614		28.3	
PBC⊥	1.523	0.111	26.7	5.5

seen on the PBC∥ profile, indicating two porous layers imbedded into the matrix of PS-PVP. They are separated by a 9.7-nm-thick "barrier" dense layer with ρ of ca. 9.5×10^{-6} Å^{-2}. We attribute these porous layers to the locations of the cylindrical channels which appear upon rinsing the SMA∥ film in methanol. The first porous layer is 6.2 nm thick and 10 nm away from the substrate. Another difference between SMA∥ and PBC∥ profiles is the thickness of the entire film. The thickness of the film decreases from 39.7 nm for SMA∥ to 37.7 nm for PBC∥. We attribute this contraction of the layer to relaxation of PBC∥, which occurs in porous polymer films. Below we reconstruct the fine structure of SMA∥ using information obtained from analysis of SMA∥ and PBC∥ samples.

Thus, X-ray reflectometry gave direct evidence for the formation of a porous stratified structure of PBC∥ films due to extraction of HABA from SMA∥. Also, it proved the parallel alignment of cylinders and allowed us to find the location of the cylinder layers in the SMA∥ film. Another technique we used to characterize the SMA and PBC films was ellipsometry. The ellipsometric thickness of the entire SMA and PBC films was in perfect agreement with X-ray reflectivity (Table 1). We used ellipsometric data for evaluation of the integral porosity of the PBC films. It is well known that analysis of ellipsometric angles Δ and Ψ allows one to calculate both the thickness and the refractive index using the fitting procedure which is usually successful for polymer
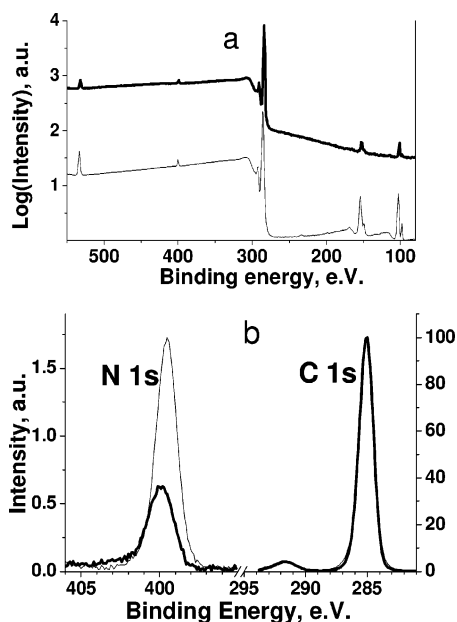
Figure 2. XPS spectra of SMA‖ (thick lines) and PBC‖ (thin lines) recorded at normal detector angle: the survey (a) and detailed spectra (b).

films thicker than 20 nm. As in the case of the X-ray reflectivity experiments, hollow channels in PBC provide sufficient contrast to measure the fraction of pores using refractive indices obtained by fitting ellipsometric data. Therefore, using the ellipsometric data we estimate the fraction of HABA which has been washed out from the SMA films. Taking into account the amount of HABA added into the composition (17.8%) and the density of the PVP+HABA complex (1.10 g/cm³),[38] we obtain a volume pore fraction in the PBC film of 0.168. Using eq 1 with $\nu_{air} = 0.168$, $n_{air} = 1.00$, and a refractive index of PS-PVP $n_{BC} = 1.59$,[37] we obtain the refractive index of the PBC film equal to 1.49.

We evaluated refractive indices of the SMA‖ ($n_{SMA‖}$) and corresponding PBC‖ samples ($n_{PBC‖}$) using ellipsometric data and compared the results with the data obtained from X-ray reflectometry experiments. The results are presented in Table 1. SMA‖ demonstrates $n_{SMA‖}$ values sufficiently higher than those of PS and PVP due to the presence of HABA in the minor block ($n_{SMA‖} = 1.616 \pm 0.01$); $n_{PBC‖}$ gives clear evidence of the porous structure after HABA extraction ($n_{PBC‖} = 1.523 \pm 0.01$). The obtained $n_{PBC‖}$ value corresponds to 0.11 volume fraction of pores, according to Bruggeman's model (eq 1). Integration of the PBC‖ profile (Figure 1) results in essentially the same porosity of 0.108. There is an apparent disagreement between the porosity (0.186) predicted from the content of HABA in the equimolar complex with the diblock copolymer and the values obtained from ellipsometric and X-ray reflectivity data. However, the thickness of the SMA‖ film decreases after HABA extraction, as documented with both ellipsometry and X-ray reflectivity techniques. Indeed, the 6.5% thickness loss (40.1 nm for SMA‖ and 37.5 nm for PBC‖) means the decrease in the porosity of 0.065, which explains the apparent discrepancy between the predicted and measured pore fractions.

The morphology of parallely aligned cylinders suggests a periodic structure. In the case of PS-PVP amphiphilic diblock copolymer, one may expect the presence of PS on the polymer−air interface because of the lower value of the surface tension of PS. However,

Table 2. Nitrogen to Carbon Ratio $\varphi_{N1s/C1s}$ of the SMA with Parallel and Perpendicular Cylinder Alignments Before and After HABA Extraction As Revealed by XPS at Normal (0°) and Grazing (60°) Detector Angles and Theoretically Calculated for the Uniform Component Distribution

	$\varphi_{N1s/C1s}{}^{a}$	$\varphi_{N1s/C1s}$ at $0°^{b}$	$\varphi_{N1s/C1s}$ at $60°^{b}$	$\lesssim^{60}\varphi_{N1s/C1s}/\varphi^{0}{}_{N1s/C1s}{}^{b}$
SMA‖	0.0306	0.0077	0.0027	0.35
PBC‖	0.0118	0.0176	0.0165	0.94
SMA⊥	0.0306	0.0150	0.0068	0.45
PBC⊥	0.0118	0.0146	0.0128	0.88

[a] Calculated from the chemical composition. [b] Obtained from XPS.

X-ray reflectometry of the PBC‖ film reveals a topmost layer of low density. This layer is about two times thicker than expected for a layer of cylindrical domains. To explain this result we performed a detailed analysis of the chemical composition of the SMA‖ surface using XPS. The survey X-ray photoemission spectra of SMA‖ and the corresponding PBC‖ samples are shown in Figure 2a. The surface chemistry of both films is represented by carbon (C1s, 285 eV) and nitrogen (N1s, 399 eV). Also, the trace amounts of silicon (Si2s, 150 eV, Si2p, 100 eV) originating from the substrate and contamination of silicon dust appear in the spectra due to imperfections of the layers. The oxygen signal (O1s, 530 eV) is useless for our purposes because it is a sum of the signals of the oxygen of HABA and the native SiO₂ layer of the silicon substrate. Thus, we concentrated on analysis of the carbon and nitrogen signals. The details of the XPS spectra of SMA‖ and PBC‖ acquired at detector angles $\theta = 0°$ and $60°$ are shown in Figure 2b. The results of the calculation of the area ratios of C1s and N1s peaks are summarized in Table 2.

The following nitrogen/carbon atomic ratios were calculated based on the chemical structures

$$\varphi_{PS} = 0$$

$$\varphi_{PVP} = 1(N1s)/7(C1s) = 0.143$$

$$\varphi_{PS-PVP} = \frac{1(N1s)_{PVP}}{7(C1s)_{PVP} + \mu_{PS/PVP}8(C1s)_{PS}} = 0.0118$$

where $\mu_{PS/PVP} = 9.74$ is the molar ratio of PS and PVP in the block copolymer

$$\varphi_{SMA} = \frac{2(N1s)_{HABA} + 1(N1s)_{PVP}}{7(C1s)_{PVP} + 13(C1s)_{HABA} + \mu_{PS/PVP}8(C1s)_{PS}}$$

taking into account the equimolar composition of PVP and HABA in the assembly.

The experimental ratio N1s/C1s in SMA‖ film at normal detector angle $\theta = 0°$ amounts to 0.0077 and is about 4 times less than that predicted for SMA composition for a homogeneous distribution of the components ($\varphi_{SMA} = 0.0306$) (Table 2). The change of the detector angle θ to grazing (60°) results in a further drastic decrease in the N1s/C1s ratio. It gives clear evidence that the topmost layer of PVP+HABA cylinders is covered with a thin layer of PS. On the other hand, a similar two-angle XPS analysis of PBC‖ sample reveals a sufficient excess of PVP on the surface φ_{PS-PVP} as compared with the case of the homogeneously distrib-
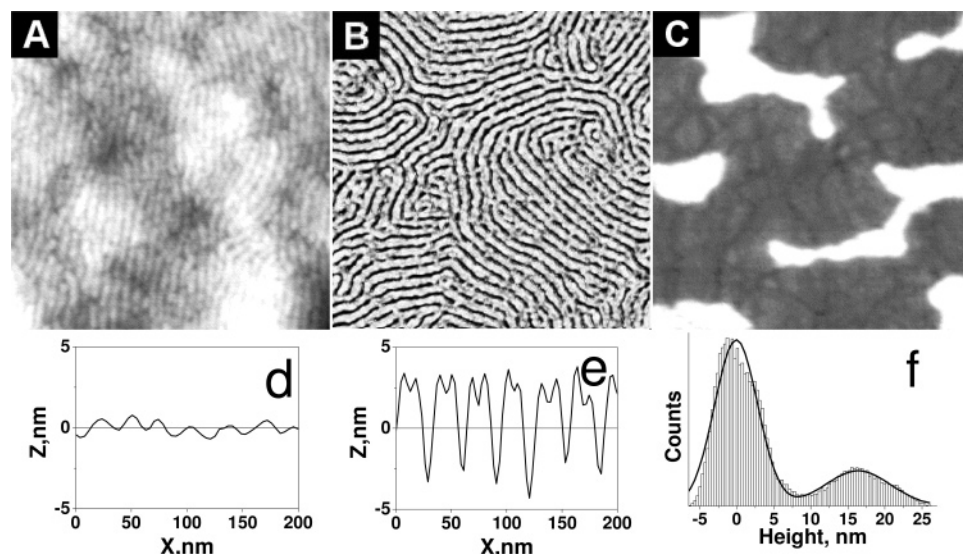
Figure 3. AFM images (height) of SMA‖ (a, 1 μm scan) and PBC‖ (b, 1 μm scan, c, 20 μm scan) samples with the corresponding cross-sections for SMA‖ (d) and PBC‖ (e), and height histogram for PBC‖ (f).

uted PVP (Table 2) independent of the θ value. It gives a strong argument that cylinders of the minor component PVP+HABA are buried into the PS matrix. They are unveiled during HABA extraction and transformed into the channels. Indeed, the interior side of the channels is covered with PVP, and the uncapping of the channels leads to an increase of the N1s signal. On the basis of the XPS experiments we explain the difference in the thickness of the first and second layers of cylinders, obtained from X-ray reflectivity, by the rupture of the upper dense PS layer during HABA extraction. We believe that extraction of HABA results in distortion of the upper dense layer in such a way that the upper layer of channels becomes open. This results in a sufficient decrease in the electron density of the upper layer appearing on the X-ray reflectivity profile of the PBC‖ sample.

We performed a detailed analysis of the surface of SMA‖ and PBC‖ samples with AFM. Comparison of two samples (Figure 3) reveals dramatic changes of the upper interface which occur during HABA extraction. The SMA‖ surface is essentially smooth at small lateral scale (1 μm), and only low-amplitude (~1 nm) ripples appear. In contrast, the PBC‖ surface demonstrates deep grooves of fingerprint-like patterns. We associate the grooves with the cylinders of PVP+HABA aligned parallel to the surface plane and transformed in the channels when HABA is removed. The power spectral density plot obtained by radial integration of the FFT images of PBC‖ is shown in Figure 4. The peak positioned at 30.7 nm reflects the in-plane periodicity of the sample. We denote it further as spatial periodicity S of the cylinders. We applied the GISAXS technique to measure S over the large sample surface. The profile of out-of-plane scattering of PBC‖ is shown in Figure 4. Although laterally resolved features are shown by a low-intensity wide peak, the multifunctional Gaussian analysis allows us to find the exact peak position at the in-plane wave vector $q_y = 0.1981$ nm^{-1}, which corresponds to $S = 31.7$ nm. Thus, the results of GISAXS measurements of the PBC‖ sample are in good agreement with the AFM data.

It is noteworthy to comment on the reproducibility of SMA‖ samples morphology, particularly the spatial periodicity of cylinders. The S value critically depends
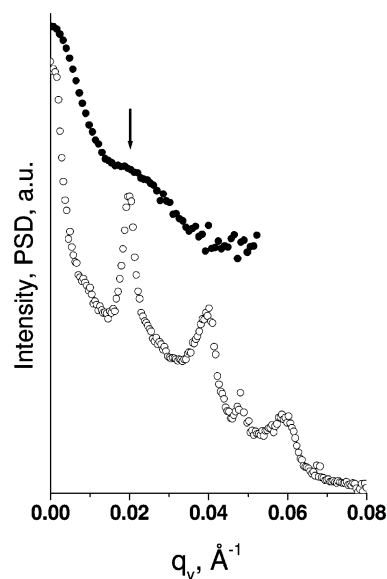
Figure 4. Power spectral density plot calculated for 1×1 μm^2 AFM image (open circles) and GISAXS out-of-plane intensity profile (filled circles) of PBC‖. The arrow shows the position of the first-order peak corresponding to the spatial periodicity of 31 nm.

on the completeness of HABA complexation. The samples obtained from a fresh solution of HABA and PS-PVP in 1,4-dioxane followed by vapor annealing in chloroform demonstrate a decrease in the S value down to 24 nm. It is accompanied by the formation of crystals of HABA appearing on the surface of the samples after vapor annealing. However, the solution aging overnight allows one to accomplish assembly formation and thus overcome the HABA macrophase separation. The samples of SMA‖ deposited from the aged solution and then swollen in chloroform vapors to a ratio of 2.75 demonstrate S in the range from 29.5 to 32 nm.

The apparent depth of the grooves is of ca. 6 nm and obviously underestimated. Indeed, the width of the grooves is ca. 7 nm, while the AFM tip diameter is at least 3 times larger. Thus, direct observation of the bottom of the grooves is impossible with the AFM tip. We identify the fingerprint-like layer as a depleted upper layer on the profile obtained with X-ray reflec-
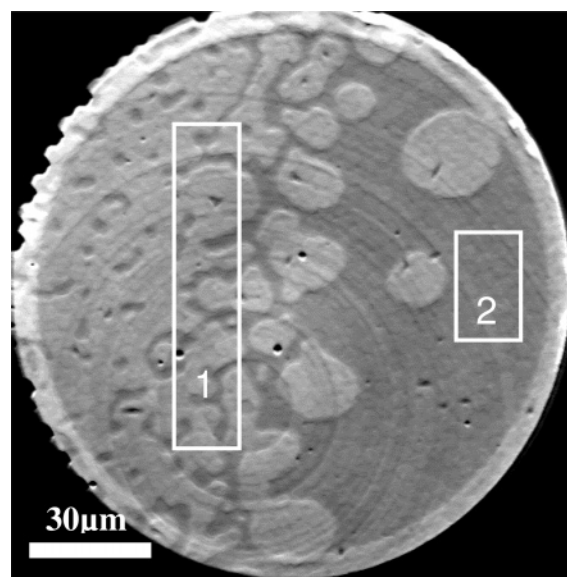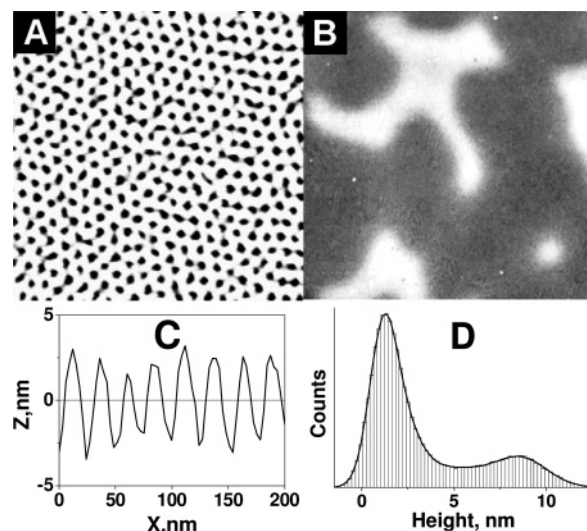
Figure 5. PEEM image (mercury lamp illumination, 4.9 eV) showing terraces on SMA∥ surface and N1s-NEXAFS spectra integrated over the surface of the upper (Field 1) and lower (Field 2) terraces. Both spectra are identical.

Figure 6. AFM images of PBC⊥ (500 nm scan, a, and 15 μm scan, b) with the cross-section (c) and height histogram (d).

Figure 7. Power spectral density plot calculated for 1×1 μm² AFM image (open circles) and GISAXS out-of-plane intensity profile (filled circles) of PBC⊥. The arrows show positions of the first (1) and higher order ($\sqrt{3}$, $\sqrt{7}$, $\sqrt{9}$) peaks. The first-order peak corresponds to spatial periodicity of 25.5 nm.
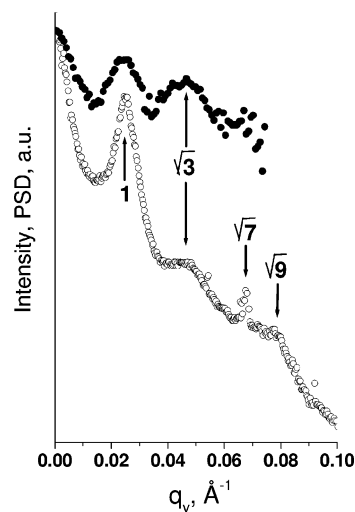
tivity (Figure 1). Therefore, combination of the X-ray reflectivity, AFM, and XPS data allows us to conclude that the distance between the center of two layers of cylinders is ca. 16 nm. We denote this value as the interlayer distance $L_{PBC\parallel}$ of the PBC∥ layer.

A large-scale imaging with AFM reveals terraces on the surface of both PBC∥ and SMA∥ samples (Figure 3c). The histogram analysis of the images shows a slight difference in the terrace height of SMA∥ and PBC∥. The surface of PBC∥ sample reveals 16.1 nm high terraces, which is in good agreement with the $L_{PBC\parallel}$ defined as described above. Meanwhile, SMA∥ surface analysis shows 17.3 nm terraces. We explain this apparent discrepancy by the relaxation effect. Indeed, the 7% difference in the heights of the terraces agrees well with the loss of the entire film thickness upon extraction as found with ellipsometry and X-ray reflectivity. It is worth noting that terracing significantly decreases the sensitivity of the reflectivity measurements, reducing the number and depth of the Kiessig fringes. Thus, we selected a 40-nm-thick SMA∥ sample for X-ray reflectometry which reveals almost no terraces.

We used XPEEM/μNEXAFS to analyze the surface composition of SMA∥ terraces. XPEEM reveals no contrast at the N1s energy (399 eV). However, UV PEEM setup allows one to visualize terraces (Figure 5) due to excitation energies close to the threshold.[39] The simultaneous μNEXAFS measurements at the lower and upper terraces in the proximity of C1s (not shown) and N1s absorption energies are almost identical. This indicates the identity of the chemical composition of the surface of both kinds of the terraces and infers completeness.

Perpendicularly Aligned C Morphology. The layer of SMA⊥ is very smooth and shows no features of nanometer scale as observed with AFM. However, extraction of HABA results in clearly seen caves arranged in a hexagonal lattice (Figure 6a and c). Fourier analysis of the AFM images of PBC⊥ samples allows calculation of the power spectral density plot (Figure 7). A prominent peak at 25.5 ± 1.5 nm is responsible for the periodicity of the caves. The GISAXS measurement of the PBC⊥ layer reveals a series of peaks at the out-of-plane scattering profile (Figure 7). The first peak of the out-of-plane wave vector $q_y = 0.246$ nm^{-1} corresponds to the 25.5 nm spatial periodicity $S_{PBC\perp}$. The clearly visible second- and third-order peaks reflect the hexagonal packing of the features according to the q_y-
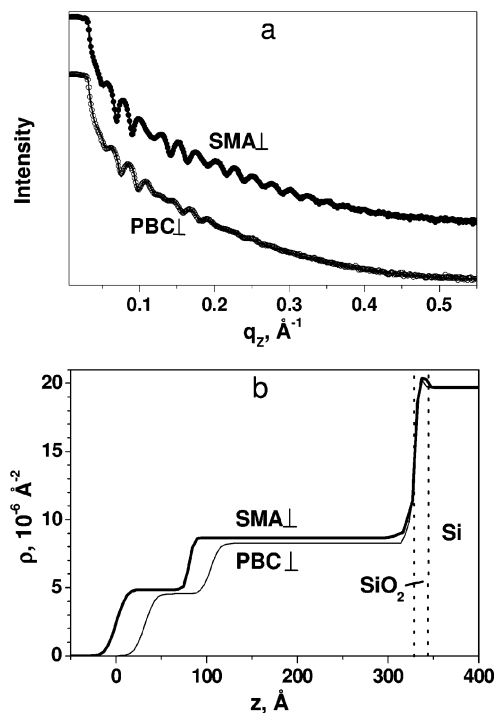
Figure 8. Measured (circles) and simulated (solid lines) X-ray reflectivity of SMA⊥ (filled circles) and PBC⊥ (open circles) films (a), and profiles of electron density ρ corresponding to the fit for SMA⊥ (thick line) and PBC⊥ (thin line).

value ratios $1/\sqrt{3}$ and $1/\sqrt{7}$. The values of the spatial periodicity of PBC⊥ sample obtained by AFM and GISAXS are in good agreement with SAXS results for the bulk SMA sample of the same composition (26.5 nm, see Experimental Section).

The AFM images of both SMA⊥ and PBC⊥ demonstrate micrometer-wide terraces of ca. 6−8 nm in height (Figure 6b and d). The terraces are also clearly seen with an optical microscope. Noteworthy, the terraces are developed upon vapor annealing in solvent−1,4-dioxane. In contrast, the samples "as deposited" are essentially terraceless. X-ray reflectometry of SMA⊥ layer reveals the terraces as an additional layer of lower electron density ρ (Figure 8). Depending on the apparent thickness of the layer, the terraces appear as a 7.5 ± 0.5 nm thick layer.

In contrast to the parallel alignment, extraction of HABA leads to an almost homogeneous distribution of polymer material in the direction normal to the sample plane (Figure 8). Only one exception is a dense layer adjacent to the substrate surface (Figure 8). This layer (1.5 nm in thickness) reproducibly appears in different samples of PBC⊥, and its presence is essential for the best fit of the reflectivity curves. The role of this layer will be hypothesized below in the discussion.

Comparison of the electron density profiles of SMA⊥ and PBC⊥ reveals a sufficient decrease in ρ (from 9.375×10^{-6} to 8.475×10^{-6} Å^{-2}) of both the "valley" layer and the "terrace" layer. The porosity of the "valley" layer is 0.096, as obtained from the ratio $\rho_{PBC\perp}/\rho_{SMA\perp}$. Simultaneously, the thickness of the entire film decreases by 6.5%. We also performed ellipsometric measurements of a series of SMA⊥ and the corresponding PBC⊥ samples varying in thickness from 25 to 70 nm. The following results were obtained: $n_{SMA} = 1.615 \pm 0.013$, $n_{PBC} = 1.523 \pm 0.011$, effective porosity 0.115 ± 0.015, thickness loss upon washing ca. 5.6%. Ellipsometric
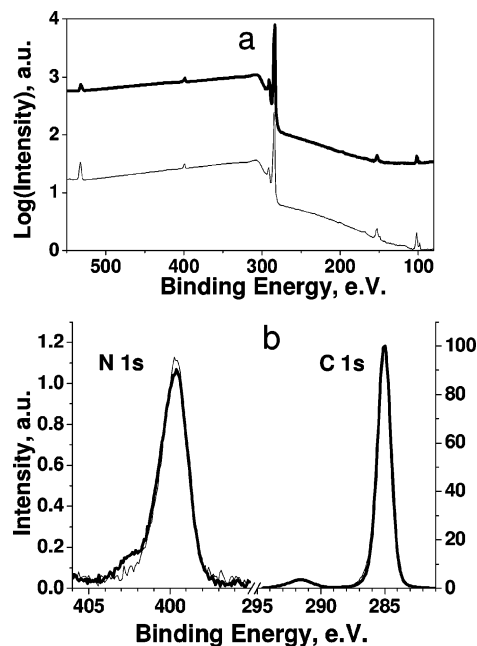
Figure 9. XPS spectra of SMA⊥ (thick lines) and PBC⊥ (thin lines) recorded at normal detector angle as survey (a) and in the N1s and C1s windows (b).

data of the samples were in good agreement with the X-ray reflectivity (Table 1). The almost constant value of the thickness loss gives additional evidence for the relaxation mechanism and homogeneous distribution of the polymer blocks in the vertical direction in PCA⊥. The thickness loss and porosity of the PBC⊥ film are in quantitative agreement with the volume fraction of HABA in SMA (0.168).

We performed two-angle XPS measurements of SMA⊥ and PBC⊥ films. The results are summarized in Table 2. The general trend remains the same as in the case of parallel alignment. SMA⊥ has a sufficiently lower fraction of nitrogen than may be predicted from the chemical composition for homogeneously distributed PVP and HABA in PS matrix. The grazing detector angle XPS gives additional evidence of a thin PS layer which covers the top of the film (Figure 9). However, the difference in φ_{SMA} measured and predicted (0.0150 and 0.0306, respectively) is not as pronounced as in the case of SMA∥. The change of the detector angle from 0° to 60° results in much lower loss of N1s signal. Both facts infer the suggestion that the PS covering layer in this case is thinner than for parallel alignment. The results obtained for PBC⊥ film demonstrate a slight excess of PVP on the surface (0.0146 at $\theta = 0°$ and 0.0128 at $\theta = 60°$ detector angle) as compared with homogeneous composition (0.0118). We explain this fact by damage of the upper PS layer upon washing, similar to the case of parallel alignment.

Discussion

One of the most intriguing points for SMA⊥ thin films is that the AFM and electron density profile suggest the perpendicular alignment of the PVP+HABA cylinders, on one hand, while optical microscopy, AFM on a larger scale, and the X-ray reflectivity profile reveal the presence of terraces, on the other. The formation of terraces is usually attributed to parallel alignment of cylinders and lamellas as well as spherical BCC morphology. Both the integral refractive index (ellipsom-
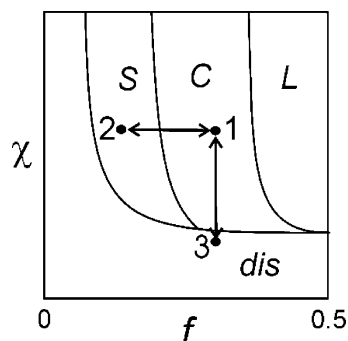
Figure 10. Left-hand part of the diagram of microphase separation in BC. Swelling in the matrix-selective solvent drives the system on the route 1 → 2, resulting in the BCC spherical morphology. On the other hand, swelling in the nonselective solvent leads to the disordered state (route 1 → 3).

Figure 11. Drying of the swollen film of parallely aligned cylinders results in the distorted hexagonal lattice.

etry) and the electron density (X-ray reflectometry) of PBC⊥ give the porosity value which is commensurate with the volume fraction of PVP+HABA minor phase estimated from the equimolar assembling of HABA to PVP (0.168). Such a volume fraction corresponds to the *C* morphology.

We explain all the facts considering the history of the samples of SMA⊥. We suggest the following scenario of the transformations of the fine structure during swelling in vapors of 1,4-dioxane and subsequent drying of SMA films. 1,4-Dioxane is a selective solvent for the SMA major component, i.e., PS.[38] According to the phase diagram of BC in selective solvent proposed by T. Lodge et al.,[40] swelling of a cylinder-forming system in a matrix-selective solvent leads to the left shift from the dry state point (Figure 10). The system undergoes the order−order transition (OOT) from a hexagonal cylindrical pattern to a BCC spherical morphology. Thus, swelling to the desired ratio (2.75 for the entire film) results in formation of the BCC spherical morphology. This process is accompanied by terrace formation. Upon the following drying a reverse morphologic transformation occurs. The vertical shrinkage of the PS matrix induces the decrease of the entire film thickness and merge of the spheres into cylinders. Moreover, BCC-packed spheres are known to be oriented in a [111] plane in thin films and appear arranged in a hexagonal lattice.[12] It makes the hexagonal packing of the cylinders even easier. The perpendicular orientation of the cylinders formed from the spheres merged in the direction normal to the surface plane is kinetically preferable. However, flattening of the SMA⊥ surface is a slow process that involves a spatial redistribution of the material, and it obviously cannot be accomplished during fast drying. The final height of the terraces on top of the dry SMA⊥ film (ca. 8 nm) is a product of the contraction of the entire swollen layer.

The analysis of the fine structure of the SMA⊥ film based on AFM, GISAXS, X-ray reflectometry, and XPS data obtained for SMA⊥ and PBC⊥ is quite simple. The layer is composed of perpendicularly oriented hexagonally packed cylinders of PVP+HABA assembly. The spatial periodicity is 25.5 nm. Taking into account the volume ratio of the minor phase (0.243), one can calculate the diameter of cylinders to be 9.3 nm. Two thin layers are adjacent to polymer−substrate and polymer−air interfaces. The lowermost polymer layer of 1.5 nm in thickness separates the substrate and the main layer of perpendicular cylinders. This layer has
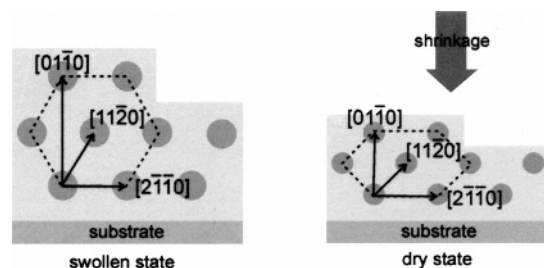
high electron density values of ca. 1.07×10^{-5} Å^{-2} for both SMA⊥ and PBC⊥ as revealed by X-ray reflectivity. The topmost layer is enriched by PS and presumably formed by a shell of spheres formerly in the swollen film. The layer is corrugated by low terraces adopted from the BCC spherical morphology and gains free energy to the system.

For the SMA‖ film the empty channels revealed by X-ray reflectometry, AFM, and GISAXS are formed upon HABA extraction from the PVP+HABA cylinders. According to the electron density profile of the PBC‖ sample, the empty channels 6.2 nm in diameter are aligned parallel to the sample plane. The distance between the first and second layers of empty channels is 9.7 nm. Therefore, the interlayer distance is 16 nm, which corresponds to a terrace layer thickness of PBC‖. Assuming the proportional contraction of the SMA‖ film of ca. 6% resulting from film relaxation, we obtain the interlayer distance $L_{SMA‖}$ = 17 nm for the PVP+HABA cylinders in SMA‖. This result agrees with the height of SMA‖ terraces (17.3 nm). However, the spatial periodicity S amounts to 31 ± 1 nm, as measured by AFM and GISAXS. Hexagonal packing suggests the factor $\sqrt{3}/2$ for the interlayer distance (Figure 11 a), giving L = 27 nm. The bulk sample and the PBC⊥ film show 26 ± 0.5 nm periodicity, which corresponds to ca. 22 nm interlayer distance. Therefore, SMA‖ film is composed of cylinders of PVP+HABA aligned parallel to the sample surface and packed in the distorted hexagonal lattice (Figure 11b). Kim and Libera[25] reported on such a distorted hexagonal lattice for the case of slow drying of a poly(styrene-*block*-butadiene-*block*-styrene) cylinder-forming block copolymer. They demonstrated a cross-sectional image of the in-plane *C* morphology obtained with TEM with the following lattice characteristics: $d[2\bar{1}\bar{1}0]$ = 40.4 nm; $d[01\bar{1}0]$ = 32.7 nm; $d[11\bar{2}]$ = 26.0 nm; lattice angles α = 39°; β = 51°.[25a] We reconstruct the following characteristics for the case of SMA‖: $d[2\bar{1}\bar{1}0]$ = 31 nm; $d[01\bar{1}0]$ = 23 nm; $d[11\bar{2}0]$ = 17 nm; lattice angles α = 42.4°; β = 47.6°. The characteristic distances are almost proportional to those obtained by Kim and Libera, and the lattice angles are similar. The closest cylinder distance, $d[01\bar{1}0]$, is ca. 10% less than that found for both the bulk and film SMA⊥ samples. This apparent disagreement can be explained by the fast drying of the samples. The parallel to sample plane orientation is reached by vapor annealing in chloroform, which is essentially a nonselective solvent for both major and minor phases of SMA. According to T. Lodge et al.,[40] swelling of cylinder-forming BC systems in neutral solvent may result in a decrease of incompatibility of the blocks (Figure 10) while the morphology pattern remains cylindrical until it reaches the order−disorder transition (ODT). On the other hand, swelling of BC may lead to an increase of

the domain spacing while fast solvent evaporation "freezes" the nonequilibrium state.[41] Currently we do not have enough data to determine if swelling to the desired ratio (2.75) brings the system into the disordered state. However, we assume that transformation of the perpendicularly oriented cylinders (as obtained from 1,4-dioxane deposition) to the parallel alignment requires the disordered state of the swollen SMA film.

Another possible scenario of perpendicular to parallel reorientation is a direct morphological transformation predicted by Suh et al.[42] and observed by Hahm et al.[43] Anyway, we consider the drying of the BC composition of hexagonally packed parallely aligned cylinders as an important factor which significantly affects the morphology and parameters of the SMA‖ film. Fast solvent evaporation results in a drastic deviation of the obtained structure from the thermodynamically stable one, i.e., disturbed hexagonal packing, as well as a decrease in the closest cylinder distance, $d[01\bar{1}0]$.

Another important feature of the SMA‖ thin films is the presence of a thin disordered layer at the polymer–substrate interface. As mentioned above, it is indicative of the preferential wetting phenomenon. Considering the electron density profile of PBC‖, the interlayer distance between the first and second cylinder layer is 9.7 nm. This space is occupied by PS shells of cylinders of the two layers. Thus, the shell effective thickness amounts to ca. 5 nm. The first layer of the cylinders is located 10 nm away from the substrate, and only 5 nm of this space is occupied by cylinder shells. We attribute another 5 nm to the layer adjacent to the substrate surface, i.e., wetting layer. The same thickness of the wetting layer can be obtained from a simple evaluation based on the AFM data. The vertical periodicity of SMA‖ film is commensurate with the terrace height (17 nm). We found the thickness of the terraceless sample to be 39 nm. Upon a gradual increase of the deposited film thickness we found that the next terraceless SMA‖ film is 56 nm thick. Therefore, we conclude that the films are constructed from a 5 nm wetting layer and two (for 39-nm-thick film) or three (for 56-nm-thick film) layers of parallel cylinders. The free polymer–air interface of SMA‖ is occupied with the PS shell of the PVP+HABA cylinders. We define the quantization relationship for the entire SMA‖ film thickness t as

$$t = n \, L_{\text{SMA}\|} + w$$

where n is the number of cylindrical layers, integer, and $w = 5$ nm is the thickness of the wetting disordered layer on the substrate surface.

The performed experiments give no direct information about the wetting layer. We can speculate that PVP blocks preferentially wet the polar surface of the substrate (Si/SiO$_2$) and PS blocks are located in the proximity of the first cylinder layer and wet the PS shell of the cylinders.

Kim and Libera[25] found for a poly(styrene-*block*-butadiene-*block*-styrene) cylinder-forming block copolymer that a very fast (free) solvent evaporation results in the poorly ordered perpendicular structure. However, an ordered perpendicular structure was obtained at about 10 times slower evaporation. Moreover, a very slow evaporation (300 times slower) allowed the parallel orientation. It is obviously not the case for the SMA. We prepared the samples using rapid ("free" drying, within a fraction of a second), slow (within 15 s), and very slow evaporation (within 10 min) in a closed chamber. In all cases we observed the same structure. The decrease of the evaporation rate resulted in sufficient order improvement for samples with a perpendicular alignment. We believe that HABA plays a crucial role in formation of the well-ordered perpendicular structure. The mechanism is under investigation in our group. Currently, we can speculate that the weak and reversible PVP+HABA assembly facilitates the nanodomain ordering due to a dynamic change in the number of HABA molecules in PVP domains and at the interfaces.

The structure of SMA⊥ is indifferent to the substrate. In addition to silicon wafers used as a standard substrate, we used silicon wafers modified with grafted PS and PVP homopolymer brushes as well as binary brushes of different composition,[24] polybutadiene films, gold and nickel substrates, and found no difference in the structure as revealed by AFM. We speculate that this indifference to the substrate surface behavior is affected by the 1.5–2-nm-thick layer at the polymer–substrate interface revealed by X-ray reflectivity. It is much thinner than layers usually observed for the wetting or disordered layer (typically about one-half of a period, see, e.g., refs 9 and 16) and significantly thinner than the wetting layer we observe in the case of SMA‖ (5 nm). We believe it plays a role of an adaptive layer leveling interfacial energies of the substrate–PS and the substrate–PVP+HABA interfaces. The adsorbed layer of PS-PVP+HABA arises at early stages of deposition due to polar–polar (in the case of SiO$_2$), nonpolar (polybutadiene film, PS brush), or donor–acceptor (gold, nickel substrates) interactions. HABA molecules compete for pyridine segments in such a way that some fraction of PVP interacts with the substrate while a part of PVP segments interacts with HABA molecules and is exposed to the polymer film. The number of exposed chains of PVP+HABA changes if the cylindrical PVP+HABA domains or PS matrix interact with the adsorbed layer in the particular location. The adsorbed layer adopts its morphology to minimize the interfacial energy. The nature and structure of the adaptive layer remain uncovered and will be the subject of a future investigation.

Conclusions

The combination of AFM, XPS, XPEEM, GISAXS, ellipsometry, and X-ray reflectometry allowed us to investigate the fine structure of thin films of the SMA. Perpendicular or parallel orientation of cylindrical nanodomains was achieved depending on the solvent used for deposition and vapor annealing of the SMA.

The parallely aligned films consist of layers of cylinders separated by PS matrix. A thin (5 nm) wetting layer is found at the polymer–substrate interface. The free surface is enriched with PS and exhibits terraces. Films of PBC demonstrate a fingerprint-like structure at the nanometer scale. Nanocylinders of PVP+HABA are packed into the distorted hexagonal lattice, exhibiting a 31 nm spatial period and a 17 nm interlayer distance. In contrast, the perpendicular alignment reveals the perfect regular hexagonal lattice with a spatial period of 25.5 nm. While SMA⊥ film is essentially smooth at the nanometer scale and covered with a very thin PS layer, extraction of HABA results in corrugation of the uppermost layer and opens the vertical channels. The channels cross the entire film down to a dense 1.5-nm-thick "adaptive" layer adjacent

to the polymer−substrate interface. We hypothesized that the adaptive layer levels the interfacial energies of the SMA components, thus allowing the perpendicular orientation.

Solvent evaporation drives the SMA structure to adopt the perpendicular orientation. 1,4-Dioxane is a solvent selective for the PS matrix. Swelling in 1,4-dioxane leads the system from cylindrical to BCC spherical morphology. Solvent evaporation results in a shrinkage of the matrix in the vertical direction and subsequently merges the spheres into the vertical cylinders.

Easy extraction of the additive from the block copolymer assembly is an advantage for simple fabrication of nanotemplates. At the same time, the porous materials obtained from SMA facilitates increasing the contrast for investigation of the morphology and self-organization in thin block copolymer films.

References and Notes

(1) Bates, F. S.; Fredrickson, G. H. *Annu. Rev. Phys. Chem.* **1990**, *41*, 525−557.
(2) Krausch, G.; Magerle, R. *Adv. Mater.* **2002**, *14*, 1579−1583.
(3) Park, M.; Harrison, C.; Chaikin, P. M.; Register, R. A.; Adamson, D. H. *Science* **1997**, *276*, 1401−1404.
(4) Hasegawa, H.; Hashimoto, T. *Macromolecules* **1985**, *18* (3), 589−590.
(5) Anastasiadis, S. H.; Russell, T. P.; Satja, S. K.; Majkrzak, C. F. *Phys. Rev. Lett.* **1989**, *62* (16), 1852−1855.
(6) Fredrickson, G. H. *Macromolecules* **1987**, *20* (10), 2535−2542.
(7) Huinink, H. P.; van Dijk, M. A.; Brokken-Zijp, J. C. M.; Sevink, G. J. A. *Macromolecules* **2001**, *34*, 5325−5339.
(8) Turner, M. S.; Rubinstein, M.; Marques, C. M. *Macromolecules* **1994**, *27* (18), 4986−4992.
(9) Liu, Y.; Zhao, W.; Zheng, X.; King, A.; Singh, A.; Rafailovich, M. H.; Sokolov, J.; Dai, K. H.; Kramer, E. J.; Schwarz, S. A.; Gebizlioglu, O.; Sinha, S. K. *Macromolecules* **1994**, *27* (14), 4000−4010.
(10) Harrison, C.; Park, M.; Chaikin, P. M.; Register, R. A.; Adamson, D. H.; Yao, N. *Macromolecules* **1998**, *31*, 2185.
(11) Yokoyama, H.; Kramer, E. J.; Rafailovich, M. H.; Sokolov, J.; Schwarz, S. A. *Macromolecules* **1998**, *31* (25), 8826−8830.
(12) Thomas, E. L.; Kinning, D. J.; Alward, D. B.; Henkee, C. S. *Macromolecules* **1987**, *20* (11), 2934−2939.
(13) Green, P. F.; Limary, R. *Adv. Colloid Interface Sci.* **2001**, *94*, 53−81.
(14) Coulon, G.; Russell, T. P.; Deline, V. R.; Green, P. F. *Macromolecules* **1989**, *22* (6), 2581−2589.
(15) Russell, T. P.; Coulon, G.; Deline, V. R.; Miller, D. C. *Macromolecules* **1989**, *22* (12), 4600−4606.
(16) (a) Knoll, A.; Magerle, R.; Krausch, G. *J. Chem. Phys.* **2004**, *120* (2), 1105−1116. (b) Horvat, A.; Lyakhova, K. S.; Sevink, G. J. A.; Zvelindovsky, A. V.; Magerle, R. *J. Chem. Phys.* **2004**, *120* (2), 1117−1126.
(17) Amundson, K.; Helfand, E.; Davis, D. D.; Quan, X.; Patel, S. S.; Smith, S. D. *Macromolecules* **1991**, *24*, 6546.
(18) Amundson, K.; Helfand, E.; Quan, X.; Smith, S. D. *Macromolecules* **1993**, *26*, 2698.
(19) Morkved, T. L.; Lu, M.; Urbas, A. M.; Ehrichs, E. E.; Jaeger, H. M.; Mansky, P.; Russell, T. P. *Science* **1996**, *273*, 931.
(20) Morkved, T. L.; Lopez, V. A.; Hahm, J.; Sibener, S. J.; Jaeger, H. M. *Polymer* **1998**, *39*, 3871.
(21) Mansky, P.; DeRouchey, J.; Russell, T. P.; Mays, J.; Pitsikalis, M.; Morkved, T. L.; Jaeger, H. M. *Macromolecules* **1998**, *31*, 4399.
(22) Thurn-Albrecht, T.; DeRouchey, J.; Russell, T. P.; Jaeger, H. M. *Macromolecules* **2000**, *33*, 3250.
(23) Böker, A.; Knoll, A.; Elbs, H.; Abetz, V.; Müller, A. H. E.; Krausch, G. *Macromolecules* **2002**, *35* (4), 1319−1325.
(24) Mansky, P.; Russell, T. P.; Hawker, C. J.; Pistikalis, M.; Mays, J. *Macromolecules* **1997**, *30* (22), 6810−6813.
(25) (a) Kim, G.; Libera, M. *Macromolecules* **1998**, *31*, 2569−2577. (b) Kim, G.; Libera, M. *Macromolecules* **1998**, *31*, 2670−2672.
(26) Kim, S. H.; Misner, M. J.; Xu, T.; Kimura, M.; Russell, T. P. *Adv. Mater.* **2004**, *16* (3), 226−231.
(27) Ruokolainen, J.; Mäkinen, R.; Torkkeli, M.; Mäkelä, T.; Serimaa, R.; ten Birke, G.; Ikkala, O. *Science* **1998**, *280*, 557−560.
(28) Mäki-Ontto, R.; de Moel, K.; de Odorico, W.; Ruokolainen, J.; Stamm, M.; ten Brinke, G.; Ikkala, O. *Adv. Mater.* **2001**, *13*, 117−121.
(29) Sidorenko, A.; Tokarev, I.; Minko, S.; Stamm, M. *J. Am. Chem. Soc.* **2003**, *125* (40), 12211.
(30) Ruokolainen, J.; Saariaho, M.; Ikkala, O.; ten Brinke, G.; Thomas, E. L.; Torkkeli, M.; Serimaa, R. *Macromolecules* **1999**, *32*, 1152−1158.
(31) Bruggeman, D. A. G. *Ann. Phys. (Leipzig)* **1935**, *24*, 636−664.
(32) Parrat, L. G. *Phys. Rev.* **1954**, *55*, 359−369.
(33) Hoffman, P.; Schmeisser, D.; Roters, G.; Nenyei, Z. *Thin Solid Films* **2003**, *428*, 216−222.
(34) Batchelor, D. R.; Follath, R.; Schmeisser, D. *Nucl. Instrum. Methods Phys. Res., Sect. A* **2001**, *470*, 467−468.
(35) Simon, F.; Jacobasch, H. J.; Spange, S. *Colloid Polym. Sci.* **1998**, *276*, 930.
(36) Moulder, J. F.; Stickle, W. F.; Sobol, P. E.; Bomben, K. D. *Handbook of X-ray Photoelectron Spectroscopy*; Perkin-Elmer Corp.: Eden Prairie, MN, 1992.
(37) Brandup, J.; Immergut, E. H.; Grulke, E. *Polymer Handbook*, 4th ed.; Wiley: New York, 1999.
(38) We prepared an assembly of PVP homopolymer and HABA dissolving a sample of PVP (M_n 3000 g/mol) in a HABA solution in 1,4-dioxane in ultrasonic bath at elevated temperature (80 °C). After keeping the solution overnight, several pieces of the assembly were obtained. The PVP+HABA assembly was almost insoluble in 1,4-dioxane and soluble in chloroform. The density of the assembly was measured by buoyancy technique in NaCl water solution. The density is 1.10 g/cm³.
(39) Mikalo, R. P.; Hoffmann, P.; Heller, Th.; Batchelor, D. R.; Appel, G.; Schmeisser, D. *Mater. Sci. Eng.* **1999**, (C8−9), 257−265.
(40) Hanley, K. J.; Lodge, T. P.; Huang, C.-I. *Macromolecules* **2000**, *33* (16), 5918−5931.
(41) Böker, A.; Elbs, H.; Hänsel, H.; Knoll, A.; Ludwigs, S.; Zettl, H.; Zvelindovsky, A. V.; Sevink, G. J. A.; Urban, V.; Abetz, V.; Müller, A. H. E.; Krausch, G. *Macromolecules* **2003**, *36*, 8078−8087.
(42) Suh, K. Y.; Kim, Y. S.; Lee, H. H. *J. Chem. Phys.* **1998**, *108*, 1253.
(43) Hahm, J.; Sibener, S. J. *J. Chem. Phys.* **2001**, *114*, 4730−4740.